Available online at www.sciencedirect.com

ScienceDirect

www.elsevier.com/locate/jes

JES JOURNAL OF ENVIRONMENTAL SCIENCES

www.jesc.ac.cn

Potential of secondary aerosol formation from Chinese gasoline engine exhaust

Zhuofei Du[1], Min Hu[1,], Jianfei Peng[1], Song Guo[1], Rong Zheng[2], Jing Zheng[1], Dongjie Shang[1], Yanhong Qin[1], He Niu[1], Mengren Li[1], Yudong Yang[1], Sihua Lu[1], Yusheng Wu[1], Min Shao[1], Shijin Shuai[2]*

1. *State Key Joint Laboratory of Environmental Simulation and Pollution Control, College of Environmental Sciences and Engineering, Peking University, Beijing 100871, China*
2. *State key Laboratory of Automotive Safety and Energy, Department of Automotive Engineering, Tsinghua University, Beijing 100084, China*

ARTICLE INFO

Article history:
Received 1 September 2016
Revised 17 February 2017
Accepted 22 February 2017
Available online 20 April 2017

Keywords:
Port fuel injection
Gasoline engine exhaust
Secondary aerosol formation
Chamber simulation
Secondary organic aerosol

ABSTRACT

Light-duty gasoline vehicles have drawn public attention in China due to their significant primary emissions of particulate matter and volatile organic compounds (VOCs). However, little information on secondary aerosol formation from exhaust for Chinese vehicles and fuel conditions is available. In this study, chamber experiments were conducted to quantify the potential of secondary aerosol formation from the exhaust of a port fuel injection gasoline engine. The engine and fuel used are common in the Chinese market, and the fuel satisfies the China V gasoline fuel standard. Substantial secondary aerosol formation was observed during a 4–5 hr simulation, which was estimated to represent more than 10 days of equivalent atmospheric photo-oxidation in Beijing. As a consequence, the extreme case secondary organic aerosol (SOA) production was 426 ± 85 mg/kg-fuel, with high levels of precursors and OH exposure. The low hygroscopicity of the aerosols formed inside the chamber suggests that SOA was the dominant chemical composition. Fourteen percent of SOA measured in the chamber experiments could be explained through the oxidation of speciated single-ring aromatics. Unspeciated precursors, such as intermediate-volatility organic compounds and semi-volatile organic compounds, might be significant for SOA formation from gasoline VOCs. We concluded that reductions of emissions of aerosol precursor gases from vehicles are essential to mediate pollution in China.

Introduction

After a tremendous increase in recent years, the total quantity of vehicles in China reached 269 million in 2015, comprising the second largest vehicle population in the world (National Bureau of Statistics of China, 2015). Vehicles emit large amounts of particulate matters and gaseous pollutants, such as carbon monoxide, nitrogen oxides and volatile organic compounds (VOCs). Primary particles from vehicles have been reported to contribute 5%–10% of $PM_{2.5}$ (particulate matter with diameter less than 2.5 μm) in megacities in China (Huang et al., 2014). Gaseous pollutants from vehicles are precursors to secondary aerosols through gaseous- and/or aqueous-phase oxidation in the atmosphere (Gentner et al., 2012).

Previous smog chamber studies of exhaust from light-duty gasoline engines/vehicles have demonstrated that the amount of secondary aerosol formed from the oxidation of gaseous precursors exceeds that of primary aerosols emitted directly

* *Corresponding author*. E-mail: minhu@pku.edu.cn (Min Hu).

http://dx.doi.org/10.1016/j.jes.2017.02.022
1001-0742/

(Jathar et al., 2014). These studies, however, were based on standards and usage data for gasoline engines and vehicles in Europe. Little information on secondary aerosol formation based on China's gasoline vehicle emissions is available in the literature. The complexity and uncertainty regarding the mechanisms of secondary aerosol formation have led to the poor understanding of the contribution of light-duty gasoline vehicles to ambient $PM_{2.5}$.

Secondary aerosols, mainly organics, nitrate, sulfate and ammonium, account for large fractions of PM_1 in many mega cities of China: 51%–80% in Beijing, 72%–84% in Shanghai and 77%–83% in Guangzhou (Huang et al., 2010, 2012). They drive severe haze pollution events to a large extent. However, the sources of secondary aerosols are not well-known, due to the lack of understanding of their composition and formation mechanisms (Hallquist et al., 2009; Guo et al., 2012). Some scholars have combined factor analysis with ^{14}C analysis to distinguish fossil and non-fossil sources of secondary organic aerosol (SOA) (Szidat, 2009). Fossil SOA, mainly from traffic and coal burning, has been found to contribute about 45%–65% of SOA in Beijing (Huang et al., 2014), indicating the significant contribution of vehicles to SOA in urban areas.

In this study, a series of chamber experiments was conducted to investigate secondary aerosol formation from gaseous pollutants in gasoline engine exhaust. The port fuel injection (PFI) gasoline engine and fuel tested both have major market share in China. Diluted gaseous pollutants were injected into an outdoor chamber and photo-oxidized to examine secondary aerosol formation. This study was conducted to link vehicle source emissions with ambient particle matter, with the aims of evaluating the potential of secondary aerosol formation from gasoline engine exhaust in the ambient atmosphere, improving the general understanding of secondary aerosol formation mechanisms, and promoting reconceptualization of the role of gasoline vehicle emissions in atmospheric aerosol pollution.

1. Materials and methods

1.1. Experimental set-up

Primary emissions of gaseous pollutants and particles were measured at the engine tailpipe using the gas analyzer AVL Combustion Emissions Bench II (CEB II, AVL, Austria). Particle samples from the engine tailpipe were analyzed by a balance and organic carbon/elemental carbon analyzer (OC/EC analyzer, Sunset Lab, USA), and primary emission factors were calculated accordingly.

The secondary aerosol formation simulation experiments were carried out in the outdoor chamber in September 2014 in Beijing. The two-layer outdoor chamber has a volume of 1.2 m^3. The inner layer is made of 0.13 mm perfluoroalkoxy (PFA) Teflon and the outer layer is a 5.6 mm thick rigid acrylic shell (OP-4 Acrylite, Cyro Industries, USA). Ambient sunlight is used to generate reactions in the chamber, in an environment similar to the real atmosphere. OP-4 Acrylite and PFA Teflon allow efficient ultraviolet (UV) transmission in the UV-B (280–315 nm) and UV-A (315–400 nm) ranges, leading to the penetration of about 60% of UV light through the two-layered wall into the chamber.

Four chamber experiments were performed with a PFI engine and fuel with 28.5% aromatic hydrocarbons, complying with China V gasoline fuel standard. The engine functioned at 2000 r/min and 50% loading. The experimental conditions are listed in Table 2.

Prior to each experiment, the chamber was cleaned by flushing with zero air for about 35 hr and illuminating with sunlight, to create a pristine environment. It was then covered with two layers of anti-UV cloth to block sunlight. Engine exhaust was injected into the chamber through a heater. Samples were heated up to 200°C, to reduce VOC loss. The particles in the exhaust were filtered, to ensure that the initial particle concentration was <100 particles/cm^3. Excess (1 mL, 30%) H_2O_2 was also injected to generate sufficient OH exposure. Ambient sunlight was used to induce H_2O_2 to produce OH radicals. OH exposure in the chamber was calculated from the photolysis of H_2O_2, using actinic flux spectra recorded by a multi-channel spectrometer with a photodiode array (Carl Zeiss MicroImaging GmbH, Germany). The related theory and details of physical and chemical processes were described by Stark et al. (2007). Assuming the 24 hr mean concentration of 10^6 OH molecules/cm^3 in Beijing (Lu et al., 2013), the OH exposure at the end of the experiments simulated an almost extreme case of oxidation, corresponding to more than 10 days in the atmosphere. Fig. 1 is a schematic illustration of the outdoor chamber, and the injection and measurement set-up.

After the injection of gaseous pollutants and H_2O_2, a 15-minute period was allowed to ensure sufficient mixing, and primary emissions in the dark chamber were then characterized. The anti-UV cloth was then removed to initiate photo-oxidation, this timepoint was referred to as t = 0 hr (Fig. 2). All experiments were conducted from about 13:00 to 17:00 with differing sunlight intensity.

High time resolution instruments were used to characterize gaseous and particulate-phase samples inside the chamber. VOC samples were collected from the gasoline engine exhaust

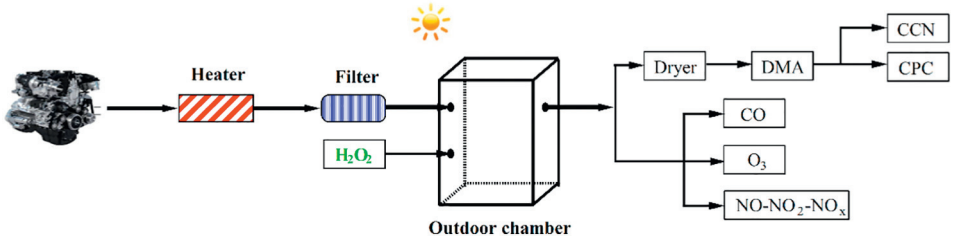

Fig. 1 – Schematic representation of the outdoor chamber set-up for the experiments. DMA: differential mobility analyzer; CPC: condensation particle counter; CCN: cloud condensation nuclei counter.

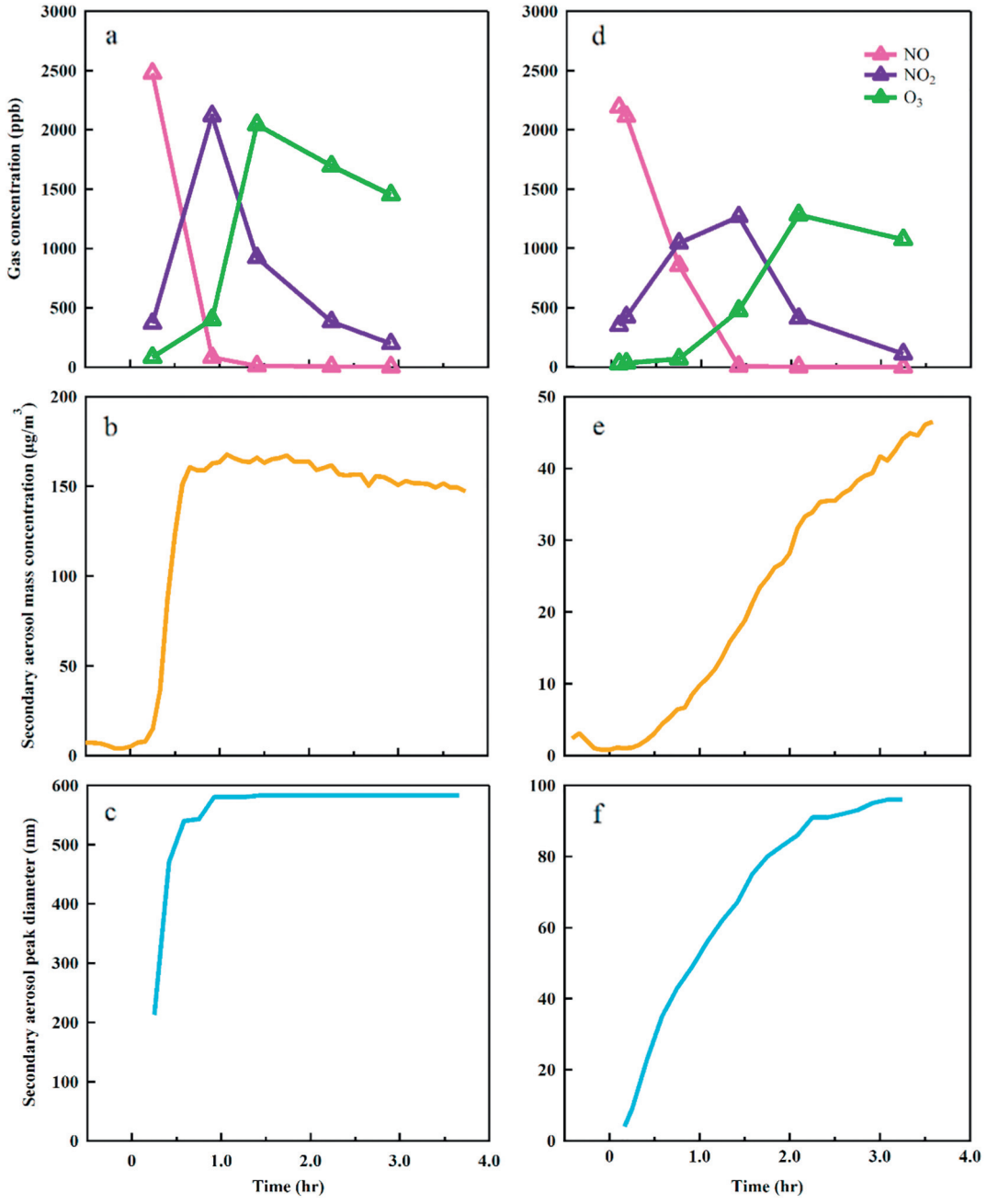

Fig. 2 – Time-resolved data for gases and particles during experiments 1 (a, b, c) and 4 (d, e, f).

using canisters, under the same mode used for the chamber experiments, and analyzed in the laboratory using gas chromatography/flame ionization detection and gas chromatography–mass spectrometry (GC/FID–GC/MS, Agilent Technologies, USA).

1.2. *Instrumentation*

To track the evolution of secondary aerosol formation in the chamber, the properties of gaseous pollutants and particles were measured simultaneously with on-site instruments. These properties included gas concentration, particle size distribution, particle mass and particle hygroscopicity. Table 1 lists the main instruments used in the experiments.

1.2.1. *Gaseous pollutant measurements*

The concentrations of CO, NO_x (including NO and NO_2) and O_3 were monitored during the aging process using CO analyzer, NO-NO_2-NO_x analyzer, and O_3 analyzer respectively.

GC/FID–GC/MS was used to measure the main VOC concentrations. The custom-built two-column system consisted of a gas chromatograph with a flame ionization detector and a quadrupole mass spectrometer with a preconcentration system (Entech 7100A, Entech Instruments, USA). One column measured C2–C4

Table 1 – Overview of main instruments used in the experiments.

Parameter	Phase	Instrument	Manufacturer	Note
CO concentration	Gas	48i CO analyzer	Thermo Fisher Scientific Inc., USA	On-line
NO, NO_2, and NO_x concentration	Gas	42i NO-NO_2-NO_x analyzer	Thermo Fisher Scientific Inc., USA	On-line
O_3 concentration	Gas	49i O_3 analyzer	Thermo Fisher Scientific Inc., USA	On-line
VOCs concentration	Gas	GC/FID-GC/MS	Agilent Technologies Inc., USA	Off-line
Aerosol number (mass) size distribution	Particle	SMPS (3081-DMA and 3775-CPC), nano-SMPS (3085-DMA and 3776-CPC)	TSI Inc., USA	On-line
Number concentration of cloud condensation nuclei	Particle	CCN (CCN-200)	Droplet Measurement Technologies Inc., USA	On-line
$PM_{2.5}$	Particle	Balance (AX105DR)	Mettler Toledo Inc., Switzerland	Off-line
OC/EC concentration	Particle	OC/EC analyzer	SUNSET Laboratory Inc., USA	Off-line
Photolysis	–	Actinic flux spectra	Carl Zeiss MicroImaging GmbH Inc., Germany	On-line

GC/FID-GC/MS: gas chromatography–flame ionization detection and gas chromatography–mass spectrometry; SMPS: scanning mobility particle sizer; DMA: differential mobility analyzer; CPC: condensation particle counter; CCN: cloud condensation nuclei counter; OC/EC: organic carbon/elemental carbon; VOCs: volatile organic compounds.

hydrocarbons and the other measured C4–C12 alkanes, C4–C11 alkenes and C6–C10 aromatics (Shao et al., 2009).

1.2.2. Particle number distribution

Scanning mobility particle sizer (SMPS) and nano-SMPS systems were used to characterize particle size distribution and mass. The SMPS system consisted of a differential mobility analyzer (DMA) and a condensation particle counter (CPC). The nano-SMPS system included nano-DMA and ultrafine-CPC. The sheath flow/aerosol flows were set as 3 L/min/(0.3 L/min) and 15 L/min/(1.5 L/min) respectively, to capture a whole particle size range of from about 3 to 700 nm. The mass concentration was calculated with consideration of number size distribution and density.

1.2.3. Particle hygroscopicity

To determine particle hygroscopicity, a dual-column cloud condensation nuclei counter (CCNc) was used to measure particle activation at a given supersaturation (SS) (Roberts and Nenes, 2005; Lance et al., 2009). The CCNc was coupled to the DMA and CPC. This system enabled the measurement of size-resolved particle activation properties. After DMA, the flow was split in two. One part was sent to the CPC, to count particle number concentration (N_{CN}), and the other part was sent to the CCNc, to count the number concentration of activated particles (N_{CCN}) (Wu et al., 2013). The activated fraction (AF) was defined as N_{CN}/N_{CCN}.

The peak diameter of particle number distribution measured by SMPS was fixed, and SS was then adjusted from low to high until the AF reached 50%. As proposed by Petters and Kreidenweis (2007), the hygroscopicity parameter κ was calculated using Eqs. (1) and (2):

$$\kappa_{CCN} = \frac{4A^3}{27D_G^3 \ln^2 SS_{50}} \quad (1)$$

$$A = \frac{4\sigma_{s/a}M_w}{RT\rho_w} \quad (2)$$

where $\sigma_{s/a}$ is droplet surface tension, M_w is the molecular weight of water, ρ_w is the density of liquid water, R is a universal gas constant, T is absolute temperature, and SS_{50} is the SS at 50% AF at a given diameter D_G.

The parameter κ was used to characterize the hygroscopicity of individual aerosol constituents, even complex aerosols in the atmosphere, based on the "κ-Kohler theory." If the particles' chemical composition changed, by chemical reactions or mixture with other compounds, κ changed (Petters and Kreidenweis, 2013). In addition, κ could be calculated as the volume-weighted average of each component's κ_i (Petters and Kreidenweis, 2007):

$$\kappa = \sum_i \varepsilon_i \kappa_i \quad (3)$$

where κ_i and ε_i are the hygroscopicity parameter and volume fraction, respectively, of component i. Thus, κ partly indicates the volume-apportioned chemical composition of secondary aerosols.

2. Results and discussion

2.1. Primary emissions

The concentrations of gaseous emissions of CO, NO_x and total hydrocarbon (THC) at the engine tailpipe were about 1167, 664 and 415 ppm C (the compound's carbon number times its volume fraction), respectively. The emission factor of non-methane organic gas (NMOG) was 2.2 g/kg-fuel, a little higher than "LEV1" gasoline vehicles (manufactured 1995–2003) in Gordon's study. The total speciated VOCs emissions constituted 78% of THC, as determined by GC/FID–GC/MS. Speciated light aromatic precursors, including benzene, toluene, and C2–C4 benzene, were classical gaseous SOA precursors (Table 3). The mass fraction of aromatic hydrocarbons accounted for about 19% of the total speciated VOCs, more than the 10%–15% for idling vehicles documented by Nordin et al. (2013), and slightly lower than the 22%–38% observed by Liu et al. (2015) for PFI vehicles. The aromatic hydrocarbon fraction of VOCs from PFI engine exhaust in this study was within the range of previous reports.

Under the mode of 2000 r/min and 50% loading, the $PM_{2.5}$ emission factor was 3.8 ± 5.4 mg/kg-fuel, with primary organic aerosol (POA) of 1.5 ± 0.2 mg/kg-fuel. The primary emission factors measured in this study are within 20% of emission factors reported in previous studies (Gordon et al., 2013, 2014a).

Our engine emitted fewer primary particles than did PFI vehicles and engines manufactured earlier, as newer engines must meet more stringent emission standards. Different testing modes may also lead to discrepancies in these measurements.

2.2. Secondary formation of gaseous pollutants from engine exhaust

The evolution of gas and particle phases in the outdoor chamber during experiment 1 is illustrated in Fig. 2. After exposure to ambient sunlight, H_2O_2 generated OH radicals. NO was converted continuously to NO_2, generating O_3 formation (Fig. 2a) (Nordin et al., 2013). In all experiments, new particle formation was observed within 15 min. The significant growth of particle diameter and mass concentration indicated substantial secondary aerosol formation (Fig. 2b and c).

Due to high initial concentrations of gaseous pollutants and OH in experiments 1, 2, and 3, wall-loss-corrected secondary aerosol mass concentrations increased rapidly after exposure to sunlight (Wall-loss correction is shown in Appendix A. Supplementary data). In experiment 1, the mass concentration increased from 6 to 170 μg/m^3 in the first 30 min (Fig. 2b). The peak diameters and the mass concentrations of secondary aerosols reached maxima within 1 hr, and remained stable in the following hours. These results indicate that secondary aerosol formation achieved extreme potential in the first hour. On the other hand, the rate of secondary aerosol formation was lower in experiment 4, in which less H_2O_2 was injected, and the particle mass concentration continued to increase until the end of the experiment (Fig. 2f).

The hygroscopicity parameter κ of 120 nm particles was 0.104 with 0.2% SS. As the concentration of SO_2 was low (<15 ppb in the chamber), we assumed that secondary aerosols consisted mostly of internally mixed ammonium nitrate and organics. The κ values of ammonium nitrate and organics (0.67 and 0.10, respectively) were applied to Eq. (3) to determine their volume-weighted averages (Svenningsson et al., 2006; Prenni et al., 2007). Organics were likely the dominant contributors to secondary aerosols formed from gaseous pollutants from gasoline engine exhaust, accounting for about 93% of these aerosols, with ammonium nitrate contributing the remaining 7%. The density of secondary aerosols was thus set as the density of organics, 1.2 g/cm^3 (Turpin and Lim, 2001).

To represent the ability of secondary aerosols to form from gaseous pollutants in gasoline engine exhaust (*i.e.*, the mass of secondary aerosols formed from gas in a unit of exhaust air), we applied Eq. (4):

$$M = \frac{(M_{max} - M_0)V_c}{V} \quad (4)$$

where M (mg/m^3) is the potential of secondary aerosol formation from gaseous pollutants in exhaust, M_{max} (mg/m^3) is the maximum particle mass concentration in the chamber during the experiments, M_0 (mg/m^3) is the initial particle mass concentration in the chamber, V_c is the volume of the chamber (1.2 m^3), and V (m^3) is the volume of exhaust air injected into the chamber.

The results of experiments 1, 2 and 3 regarding the potential of secondary aerosol formation were consistent (Table 2). The

Table 2 – Summary of conditions and results of gasoline engine exhaust experiments.

Exp No.	Date	Local time	Gasoline engine	Fuel	Operating mode	Exhaust volume (L)	Initial NO (ppb)	Initial NO_2 (ppb)	30% H_2O_2 (mL)	OH exposure	Secondary aerosol mass concentration		SOA production (mg/kg-fuel)
											Air in chamber (μg/m^3)	Exhaust (mg/m^3)	
1	September 17th	13:00–17:00	Port fuel injection	China V gasoline fuel standard	2000 r/min, 50% loading	6.0	2480	370	1	>10 day	158	31	411
2	September 19th	12:00–16:00				4.8	1836	104	1		165	41	537
3	September 24th	12:00–17:00				5.4	1946	136	1		97	25	330
4	September 15th	13:00–17:00				10.0	2190	350	<1	<10 day	45	5	70

SOA: secondary organic aerosol.

calculation of the potential of secondary aerosol formation excluded the result of experiment 4, as it was conducted with less H_2O_2 and the maximum mass concentration had not been reached at the end of experiment. After about 4 hr photo-oxidization, the average ultimate secondary aerosol mass concentration in the chamber reached 140 ± 30 μg/m^3. The potential of secondary aerosol formation reached 33 ± 6 mg/m^3 in exhaust, with SOA accounting for 30 ± 6 mg/m^3. The potential of SOA production was 426 ± 85 mg/kg-fuel.

In this study, we tried to obtain the extreme case potential of SOA production from PFI gasoline engine exhaust, with high initial gaseous pollutant concentrations and a strong oxidization environment in the chamber. However, some rather than all gaseous pollutants participated in SOA formation, because part of them was sampled by the instruments. Thus, the potential of SOA formation appears to be underestimated in this study. In addition, the semi-volatile vapors also involve some uncertainties in SOA production estimation. The loss of semi-volatile vapors to the chamber walls leads to substantial underestimation of SOA formation, by a factor of 1.1–4.1 (Zhang et al., 2014). On the other hand, the initial gas concentrations with less dilution in the chamber might lead to gas–particle partitioning into more particulate-phase during oxidation (Donahue et al., 2006).

By summarizing the chamber experiments and flow reactor simulations relative to gasoline vehicles and in-use vehicles, we find much higher SOA production in this study than in others (Fig. 3). There are two explanations for such high SOA production. First, compared with "LEV1" gasoline vehicles under the cold-start Unified Cycle driving schedule reported by Gordon et al. (2014a), the gasoline engine under 2000 r/min and 50% loading in our study emitted more VOCs per kg-fuel, contributing to higher SOA production. Second, the OH exposure in this study (equivalent to more than 10 days) was much higher than for other chamber results in most previous studies. It was reported that SOA production increased as a function of photochemical age (Tkacik et al., 2014), and our SOA production remained within the trend among other results as illustrated in Fig. 3. Tkacik et al. (2014) found that SOA production decreased after 2.7 days of OH exposure, which they attributed to a transition from functionalization- to fragmentation-dominated reaction mechanisms. In contrast, we observed no decrease in SOA production, even at more than 10 days OH exposure. This difference may be because the potential aerosol mass reactor used in Tkacik's study simulates 9 days in approximately 100 sec, with an oxidation environment greatly exceeding that of ambient air, leading to potential differences in reaction mechanisms. The contribution of intermediate-volatility organic compounds (IVOCs) and semi-volatile organic compounds (SVOCs) due to high initial gas concentrations may be another explanation.

The SOA production potential from gasoline engine obtained in this study is comparable with those from scooters and diesel vehicles without aftertreatment, but much higher than diesel vehicles with aftertreatment (Platt et al., 2014; Gordon et al., 2014b). Our result can represent emission from widely used gasoline vehicles with lower-tech aftertreatment. Considering the much larger population of gasoline vehicles in Chinese megacities such as Beijing, with over 3000 gasoline vehicles per square kilometer, this high potential implies the significant impact of gasoline emission on air quality, properly the largest among all kinds of traffic emissions in urban areas.

2.3. SOA mass closure of gasoline exhaust

The second organic aerosol yield Y was defined as the ratio of the wall-loss-corrected measured SOA mass at the end of the experiments (ΔOA) to the mass of SOA precursors (ΔVOC) (Donahue et al., 2006; Odum et al., 1996), which was calculated by Eq. (5):

$$Y = \frac{\Delta OA}{\Delta VOC} \quad (5)$$

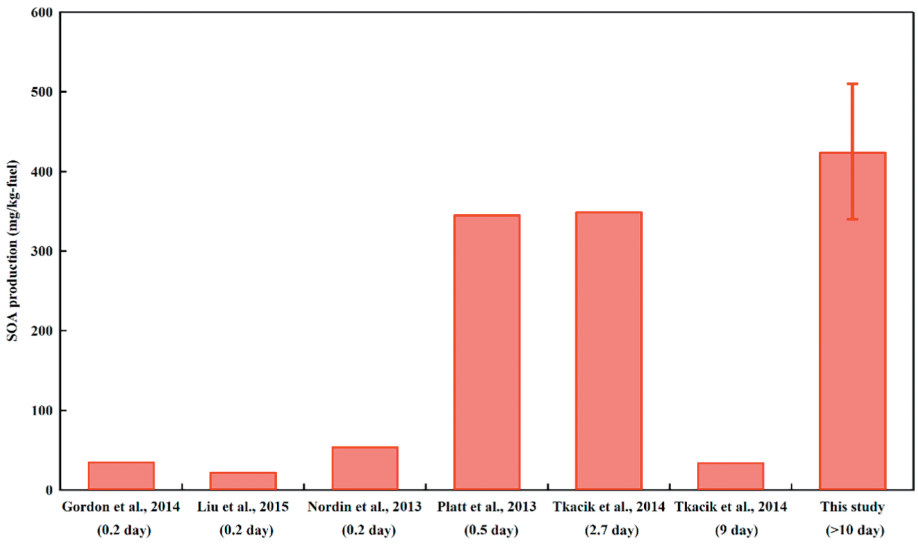

Fig. 3 – Fuel-based secondary organic aerosol (SOA) production in the present chamber study and in flow reactor studies. The times of equivalent photochemical age are marked on the x-axis labels.

SOA production ($\Delta OA_{predicted}$) from the exhaust was predicted using Eq. (6):

$$\Delta OA_{predicted} = \sum_i (\Delta_i \times Y_i) \quad (6)$$

where Δ_i is the change in VOC_i concentration and Y_i is the SOA yield of VOC_i. The concentration of VOCs, including benzene, toluene, C2–C4 benzene in exhaust, were used to estimate the SOA production.

SOA formation from the photo-oxidation of VOCs was highly sensitive to the NO_x conditions (Song et al., 2005; Ng et al., 2007a). Ng et al. (2007b) performed chamber experiments to examine SOA formation under high NO_x conditions, with NO_x concentrations of about 1 ppm at the inception of photo-oxidation. Some researchers consider VOCs/NO_x = 0.3 to represent a high NO_x condition (Metzger et al., 2008), and VOCs/NO_x > 6 to represent a low NO_x condition (Borrás and Tortajada-Genaro, 2012; Platt et al., 2013). In this study, the initial NO_x concentrations were 1.9–2.8 ppm, and the VOCs/NO_x ratio was about 0.5. Therefore, the SOA formation by gaseous pollutants from PFI engine exhaust in the chamber occurred under high NO_x conditions.

Table 3 lists SOA yields and predicted SOA concentrations of benzene, toluene, and C2–C4 benzenes, including 16 compounds measured by off-line GC–MS. High NO_x SOA yields for benzene, toluene, and *m*-xylene were taken from Ng et al. (2007b), and the SOA yield of *m*-xylene was used for C2–C4 benzenes (Platt et al., 2013). As the known SOA yields of alkanes and alkenes are much lower than those of aromatics, they were not taken into account in the SOA prediction.

The predicted SOA contributions from these VOC species are compared with SOA measured in the chamber experiments in Fig. 4. Benzene and toluene were the main precursors to SOA, in terms of concentration and yield. Predicted SOA from single-ring aromatics accounted for about 14% of the SOA production observed in the chamber experiments. This result is comparable to the 2%–12% reported by Nordin et al. (2013). Therefore, total SOA formation could not be explained by traditional speciated SOA precursors (single-ring aromatics and mid-weight VOCs), and this was also found in other fuel combustions, including wood and diesel (Weitkamp et al., 2007; Grieshop et al., 2009).

In our study, SOA from unspeciated precursors accounted for about 86% of the total measured SOA formed from exhaust of light-duty gasoline vehicles. The huge gap between predicted and measured SOA was due to the contributions of unspeciated IVOCs and SVOCs, such as branched and cyclic alkanes, and complex aromatic hydrocarbons (Robinson et al., 2007). They likely had higher molecular weights or were more polar, and thus were not captured in the GC/MS analysis in this study. Given the high initial concentrations and high SOA yield, naphthalene may be an important unspeciated precursor of SOA production, with an estimated 5%–52% contribution to SOA mass (Nordin et al., 2013; Liu et al., 2015), which is much higher than those of single-ring aromatics (Odum et al., 1997; Chan et al., 2009). When we assumed an average 29% contribution of naphthalene, the ratio of predicted to measured SOA reached about 43% in this study, comparable with the results of previous studies (Fig. 4). The SOA mass closure study indicates that unspeciated SOA precursors, including some IVOCs and SVOCs, appear to contribute the majority of SOA formation, much more than traditional SOA precursors.

Another possible explanation for the gap is the discrepancy of SOA yield under high and low NO_x conditions. The SOA yield was much higher under low NO_x conditions than under high NO_x conditions (Odum et al., 1996; Ng et al., 2007b). During 4–5 hr photo-oxidation, the NO_x condition changed from high to low (Johnson et al., 2004). Thus, the SOA yields under high NO_x conditions used to predict SOA formation will lead to underestimation in SOA prediction.

3. Conclusions

A series of experiments using an outdoor chamber was conducted to investigate secondary aerosol formation from gaseous pollutants in PFI gasoline engine exhaust. A widely

Table 3 – Predicted SOA from aromatics in this study.

Species		Emitted VOCs (ppb)	Yield	Predicted SOA (μg/(m^3 exhaust))
Benzene		1277	0.28	1141
Toluene		3761	0.11	1557
C2-benzene	Ethylbenzene	689	0.08	239
	o-Xylene	165	0.08	57
	m/p-Xylene	512	0.08	178
	Styrene	18	0.08	6
C3-benzene	1,3,5-Trimethylbenzene	359	0.08	141
	1,2,4-Trimethylbenzene	84	0.08	33
	1,2,3-Trimethylbenzene	32	0.08	13
	o-Ethyltoluene	250	0.08	98
	m-Ethyltoluene	667	0.08	262
	p-Ethyltoluene	292	0.08	114
	n-Propylbenzene	150	0.08	59
	i-Propylbenzene	45	0.08	18
C4-benzene	o-Diethylbenzene	116	0.08	51
	m-Diethylbenzene	34	0.08	15

VOC yields were taken from Ng et al. (2007b).

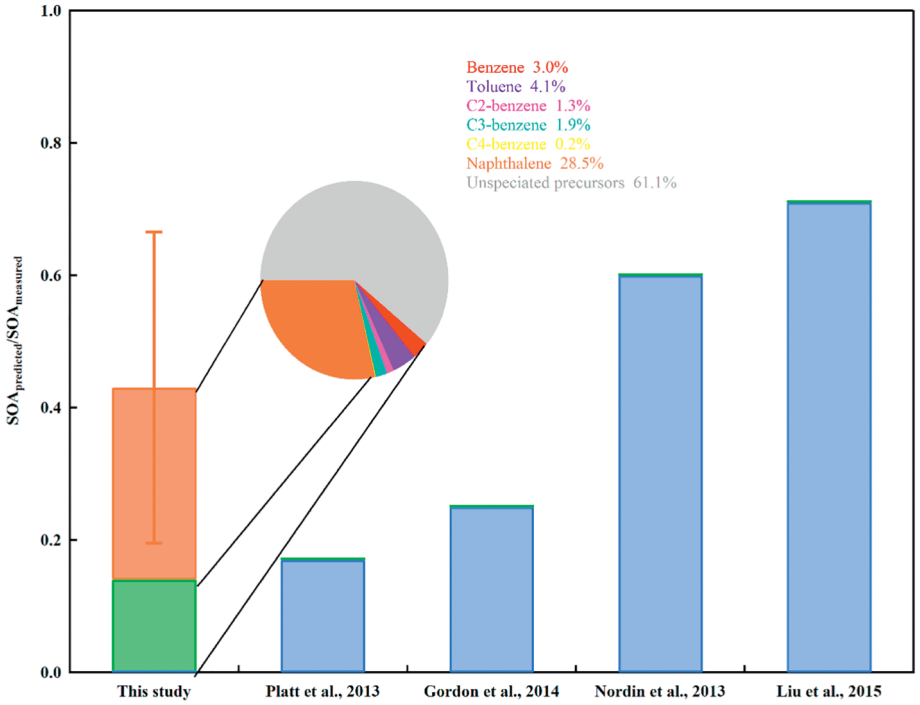

Fig. 4 – Predicted SOA production ($SOA_{predicted}$), calculated from speciated SOA precursors, and measured SOA formation ($SOA_{measured}$) in the chamber experiments.

used PFI engine and fuel were employed to reflect the exhaust of current gasoline vehicles with lower-tech aftertreatment in Beijing.

Substantial secondary aerosol formation occurred in the chamber during about 4–5 hr photo-oxidation, under conditions of high initial concentrations of gaseous pollutants and a strong oxidizing atmosphere. The experiments represented more than 10 days of oxidation in summer in Beijing. Secondary aerosols were composed predominantly of organics, as indicated by the hygroscopicity parameter κ. The potential of SOA production reached 33 ± 6 mg/m^3 in exhaust, and 426 ± 85 mg/kg-fuel. SOA production significantly exceeded POA in this case, consistent with the findings of many previous studies.

The high NO_x SOA mass yield was used to predict SOA formation for the mass closure study. Compared with the formed SOA observed in the chamber experiments, the use of traditional speciated SOA precursors evidently leads to the underestimation of SOA mass. IVOCs and SVOCs may be important candidate contributors to SOA formation.

This study revealed that the potential of secondary aerosol formation from gaseous pollutants in PFI gasoline engine exhaust greatly exceeds primary emissions. Thus, gasoline vehicles contribute significantly to aerosol loading in the ambient air, and have further impacts on air quality and human health. Strict control of gas precursors of secondary aerosols, such as the reduction of VOCs and NO_x emissions, should be considered.

Acknowledgments

This work was supported by the National Key Basic Research and Development Program (No. 2013CB228500), the National Basic Research Program (973) of China (Nos. 2013CB228503, 2013CB228502), National Natural Science Foundation of China (Nos. 91544214, 51636003), the Strategic Priority Research Program of Chinese Academy of Sciences (No. XDB05010500), and China Postdoctoral Science Foundation (No. 2015M580929). We also thank the State Key Lab of Automotive Safety and Energy at Tsinghua University for their support for the experiments.

Appendix A. Supplementary data

Supplementary data to this article can be found online at http://dx.doi.org/10.1016/j.jes.2017.02.022.

REFERENCES

Borrás, E., Tortajada-Genaro, L.A., 2012. Secondary organic aerosol formation from the photo-oxidation of benzene. Atmos. Environ. 47, 154–163.

Chan, A.W.H., Kautzman, K.E., Chhabra, P.S., Surratt, J.D., Chan, M.N., Crounse, J.D., et al., 2009. Secondary organic aerosol formation from photooxidation of naphthalene and alkylnaphthalenes: Implications for oxidation of intermediate volatility organic compounds (IVOCs). Atmos. Chem. Phys. 9 (9), 3049–3060.

Donahue, N.M., Robinson, A.L., Stanier, C.O., Pandis, S.N., 2006. Coupled partitioning, dilution, and chemical aging of semivolatile organics. Environ. Sci. Technol. 40 (8), 2635–2643.

Gentner, D.R., Isaacman, G., Worton, D.R., Chan, A.W.H., Dallmann, T.R., Davis, L., et al., 2012. Elucidating secondary organic aerosol from diesel and gasoline vehicles through detailed characterization of organic carbon emissions. Proc. Natl. Acad. Sci. U. S. A. 109 (45), 18318–18323.

Gordon, T.D., Tkacik, D.S., Presto, A.A., Zhang, M., Jathar, S.H., Nguyen, N.T., et al., 2013. Primary gas- and particle-phase emissions and secondary organic aerosol production from gasoline and diesel off-road engines. Environ. Sci. Technol. 47 (24), 14137–14146.

Gordon, T.D., Presto, A.A., May, A.A., Nguyen, N.T., Lipsky, E.M., Donahue, N.M., et al., 2014a. Secondary organic aerosol formation exceeds primary particulate matter emissions for light-duty gasoline vehicles. Atmos. Chem. Phys. 14 (9), 4661–4678.

Gordon, T.D., Presto, A.A., Nguyen, N.T., Robertson, W.H., Na, K., Sahay, K.N., et al., 2014b. Secondary organic aerosol production from diesel vehicle exhaust: impact of aftertreatment, fuel chemistry and driving cycle. Atmos. Chem. Phys. 14 (9), 4643–4659.

Grieshop, A.P., Logue, J.M., Donahue, N.M., Robinson, A.L., 2009. Laboratory investigation of photochemical oxidation of organic aerosol from wood fires 1: Measurement and simulation of organic aerosol evolution. Atmos. Chem. Phys. 9 (4), 1263–1277.

Guo, S., Hu, M., Guo, Q., Zhang, X., Zheng, M., Zheng, J., et al., 2012. Primary sources and secondary formation of organic aerosols in Beijing, China. Environ. Sci. Technol. 46 (18), 9846–9853.

Hallquist, M., Wenger, J.C., Baltensperger, U., Rudich, Y., Simpson, D., Claeys, M., et al., 2009. The formation, properties and impact of secondary organic aerosol: Current and emerging issues. Atmos. Chem. Phys. 9 (14), 5155–5236.

Huang, X.F., He, L.Y., Hu, M., Canagaratna, M.R., Sun, Y., Zhang, Q., et al., 2010. Highly time-resolved chemical characterization of atmospheric submicron particles during 2008 Beijing Olympic Games using an Aerodyne High-Resolution Aerosol Mass Spectrometer. Atmos. Chem. Phys. 10 (18), 8933–8945.

Huang, X.F., He, L.Y., Xue, L., Sun, T.L., Zeng, L.W., Gong, Z.H., et al., 2012. Highly time-resolved chemical characterization of atmospheric fine particles during 2010 Shanghai World Expo. Atmos. Chem. Phys. 12 (11), 4897–4907.

Huang, R.J., Zhang, Y., Bozzetti, C., Ho, K.-F., Cao, J.J., Han, Y., et al., 2014. High secondary aerosol contribution to particulate pollution during haze events in China. Nature 514 (7521), 218–222.

Jathar, S.H., Gordon, T.D., Hennigan, C.J., Pye, H.O.T., Pouliot, G., Adams, P.J., et al., 2014. Unspeciated organic emissions from combustion sources and their influence on the secondary organic aerosol budget in the United States. Proc. Natl. Acad. Sci. U. S. A. 111 (29), 10473–10478.

Johnson, D., Jenkin, M.E., Wirtz, K., Martin-Reviejo, M., 2004. Simulating the formation of secondary organic aerosol from the photooxidation of toluene. Environ. Chem. 1 (3), 150–165.

Lance, S., Nenes, A., Mazzoleni, C., Dubey, M.K., Gates, H., Varutbangkul, V., et al., 2009. Cloud condensation nuclei activity, closure, and droplet growth kinetics of Houston aerosol during the Gulf of Mexico Atmospheric Composition and Climate Study (GoMACCS). J. Geophys. Res. 114 (D7), 1159–1171.

Liu, T., Wang, X., Deng, W., Hu, Q., Ding, X., Zhang, Y., et al., 2015. Secondary organic aerosol formation from photochemical aging of light-duty gasoline vehicle exhausts in a smog chamber. Atmos. Chem. Phys. 15 (15), 9049–9062.

Lu, K.D., Hofzumahaus, A., Holland, F., Bohn, B., Brauers, T., Fuchs, H., et al., 2013. Missing OH source in a suburban environment near Beijing: Observed and modelled OH and HO concentrations in summer 2006. Atmos. Chem. Phys. 13 (2), 1057–1080.

Metzger, A., Dommen, J., Gaeggeler, K., Duplissy, J., Prevot, A.S.H., Kleffmann, J., et al., 2008. Evaluation of 1,3,5 trimethylbenzene degradation in the detailed tropospheric chemistry mechanism, MCMv3.1, using environmental chamber data. Atmos. Chem. Phys. 8 (21), 6453–6468.

National Bureau of Statistics of China, 2015. China Statistical Yearbook 2015, part eighteen: Transportation, post and telecommunications and software industry. available online at:. http://www.stats.gov.cn/tjsj/ndsj/2015/indexch.htm.

Ng, N.L., Chhabra, P.S., Chan, A.W.H., Surratt, J.D., Kroll, J.H., Kwan, A.J., et al., 2007a. Effect of NOx level on secondary organic aerosol (SOA) formation from the photooxidation of terpenes. Atmos. Chem. Phys. 7, 5159–5174.

Ng, N.L., Kroll, J.H., Chan, A.W.H., Chhabra, P.S., Flagan, R.C., Seinfeld, J.H., 2007b. Secondary organic aerosol formation from m-xylene, toluene, and benzene. Atmos. Chem. Phys. 7, 3909–3922.

Nordin, E.Z., Eriksson, A.C., Roldin, P., Nilsson, P.T., Carlsson, J.E., Kajos, M.K., et al., 2013. Secondary organic aerosol formation from idling gasoline passenger vehicle emissions investigated in a smog chamber. Atmos. Chem. Phys. 13 (12), 6101–6116.

Odum, J.R., Hoffmann, T., Bowman, F., Collins, D., Flagan, R.C., Seinfeld, J.H., 1996. Gas/particle partitioning and secondary organic aerosol yields. Environ. Sci. Technol. 30 (8), 2580–2585.

Odum, J.R., Jungkamp, T.P.W., Griffin, R.J., Flagan, R.C., Seinfeld, J.H., 1997. The atmospheric aerosol-forming potential of whole gasoline vapor. Science 276, 96–99.

Petters, M.D., Kreidenweis, S.M., 2007. A single parameter representation of hygroscopic growth and cloud condensation nucleus activity. Atmos. Chem. Phys. 7, 1961–1971.

Petters, M.D., Kreidenweis, S.M., 2013. A single parameter representation of hygroscopic growth and cloud condensation nucleus activity – Part 3: Including surfactant partitioning. Atmos. Chem. Phys. 13 (2), 1081–1091.

Platt, S.M., El Haddad, I., Zardini, A.A., Clairotte, M., Astorga, C., Wolf, R., et al., 2013. Secondary organic aerosol formation from gasoline vehicle emissions in a new mobile environmental reaction chamber. Atmos. Chem. Phys. 13 (18), 9141–9158.

Platt, S.M., Haddad, I.E., Pieber, S.M., Huang, R.J., Zardini, A.A., Clairotte, M., et al., 2014. Two-stroke scooters are a dominant source of air pollution in many cities. Nat. Commun. 5.

Prenni, A.J., Petters, M.D., Kreidenweis, S.M., DeMott, P.J., Ziemann, P.J., 2007. Cloud droplet activation of secondary organic aerosol. J. Geophys. Res. 112 (D10).

Roberts, G.C., Nenes, A., 2005. A continuous-flow streamwise thermal-gradient CCN chamber for atmospheric measurements. Aerosol Sci. Technol. 39 (3), 206–221.

Robinson, A.L., Donahue, N.M., Shrivastava, M.K., Weitkamp, E.A., Sage, A.M., Grieshop, A.P., et al., 2007. Rethinking organic aerosols: Semivolatile emissions and photochemical aging. Science 315 (5816), 1259–1262.

Shao, M., Lu, S., Liu, Y., Xie, X., Chang, C., Huang, S., et al., 2009. Volatile organic compounds measured in summer in Beijing and their role in ground-level ozone formation. J. Geophys. Res. 114, D00F15.

Song, C., Na, K.S., Cocker, D.R., 2005. Impact of the hydrocarbon to NOx ratio on secondary organic aerosol formation. Environ. Sci. Technol. 39 (9), 3143–3149.

Stark, H., Lerner, B.M., Schmitt, R., Jakoubek, R., Williams, E.J., Ryerson, T.B., et al., 2007. Atmospheric in situ measurement of nitrate radical (NO_3) and other photolysis rates using spectroradiometry and filter radiometry. J. Geophys. Res. 112 (D10).

Svenningsson, B., Rissler, J., Swietlicki, E., Mircea, M., Bilde, M., Facchini, M.C., et al., 2006. Hygroscopic growth and critical supersaturations for mixed aerosol particles of inorganic and organic compounds of atmospheric relevance. Atmos. Chem. Phys. 6, 1937–1952.

Szidat, S., 2009. Atmosphere sources of Asian haze. Science 323 (5913), 470–471.

Tkacik, D.S., Lambe, A.T., Jathar, S., Li, X., Presto, A.A., Zhao, Y., et al., 2014. Secondary organic aerosol formation from in-use

motor vehicle emissions using a potential aerosol mass reactor. Environ. Sci. Technol. 48 (19), 11235–11242.
Turpin, B.J., Lim, H.J., 2001. Species contributions to $PM_{2.5}$ mass concentrations: Revisiting common assumptions for estimating organic mass. Aerosol Sci. Technol. 35 (1), 602–610.
Weitkamp, E.A., Sage, A.M., Pierce, J.R., Donahue, N.M., Robinson, A.L., 2007. Organic aerosol formation from photochemical oxidation of diesel exhaust in a smog chamber. Environ. Sci. Technol. 41 (20), 6969–6975.
Wu, Z.J., Poulain, L., Henning, S., Dieckmann, K., Birmili, W., Merkel, M., et al., 2013. Relating particle hygroscopicity and CCN activity to chemical composition during the HCCT-2010 field campaign. Atmos. Chem. Phys. Discuss. 13 (3), 7643–7680.
Zhang, X., Cappa, C.D., Jathar, S.H., McVay, R.C., Ensberg, J.J., Kleeman, M.J., et al., 2014. Influence of vapor wall loss in laboratory chambers on yields of secondary organic aerosol. Proc. Natl. Acad. Sci. U. S. A. 111 (16), 5802–5807.